Poloidal Asymmetry of Toroidal Rotation Measured in ASDEX Upgrade

T. Pütterich, E. Viezzer, R. Dux, R.M. McDermott and the ASDEX Upgrade Team

Max-Planck-Institut für Plasmaphysik, EURATOM Assoc., D-85748 Garching, Germany

When investigating the H-mode edge at ASDEX Upgrade, the measurements from charge exchange recombination spectroscopy (CXRS) gave unexpected inter-ELM rotation profiles. In [1] and in the present work, these profiles are presented. The puzzling feature is a local minimum in the rotation near the electron density pedestal-top, since strong braking of the plasma is expected only at the separatrix. Thus, complicated transport or torque profiles are required in order to explain the structure of the toroidal rotation inside of the separatrix. This puzzle could be resolved if this structure, which was measured at the outboard midplane, is the result of a poloidal asymmetry and, therefore, not representative of the full flux surface. Such asymmetries are possible and even required to obtain divergence-free flows within a flux surface.

Flows on a Flux Surface

From the perpendicular force balance (Eq. 1) for a species α, the local velocity v_α is given by the difference between E_r and the diamagnetic term $-\frac{\vec{\nabla} p_\alpha}{Z_\alpha e n_\alpha}$, where p_α is the pressure, Z_α the charge, n_α the density of the species α and e the elementary charge. The perpendicular force balance is given by

$$0 = \vec{E} - \frac{\vec{\nabla} p_\alpha}{Z_\alpha e n_\alpha} + \vec{v}_\alpha \times \vec{B} \Rightarrow v_{\perp,\alpha} = \left(E_r - \frac{1}{Z_\alpha e n_\alpha} \frac{\partial p_\alpha}{\partial r} \right) \frac{1}{B_\parallel} \tag{1}$$

where $\vec{B}$ is the local magnetic field vector, $v_{\perp,\alpha}$ the velocity component perpendicular to $\vec{B}$ and $B_\parallel = |\vec{B}|$. It should be noted that $v_{\perp,\alpha}$ is different for the inner (high field side, HFS) and outer (low field side, LFS) midplane, which is the basic reason for non-zero divergence of $v_{\perp,\alpha}$ on a flux surface. This is compensated for by the parallel Pfirsch-Schlüter (PS) flows, which can be expressed as

$$v_{\parallel,PS} = \left(E_{r,LFS} - \frac{1}{Z_\alpha e n_\alpha} \left. \frac{\partial p_\alpha}{\partial R} \right|_{LFS} \right) \frac{B_{t,LFS}}{B_{p,LFS}} \left(\frac{1}{B_\parallel} - \frac{B_\parallel}{\langle B^2 \rangle} \right) \Rightarrow v_{\parallel,total} = v_{\parallel,PS} + v_{B_\parallel} \tag{2}$$

In Eq. 2 $B_{t,LFS}$, $B_{p,LFS}$, $E_{r,LFS}$, n_α and $\left. \frac{\partial p_\alpha}{\partial R} \right|_{LFS}$, denote the toroidal and poloidal magnetic field, the radial electric field, the density of the particle species α and its pressure gradient at one location on the LFS. $\langle B^2 \rangle$ is the flux surface average of B^2. $B_\parallel$ is evaluated locally.

In Fig. 1 the flow structure of PS flows for a real geometry at the radius $\rho_{pol} = 0.975$ is indicated for the condition $E_r - \frac{1}{Z_\alpha e n_\alpha} \frac{\partial p_\alpha}{\partial r} < 0\,\mathrm{kV/m}$. Blue (red) regions indicate flows directed out of (into) the plane of the paper. The thickness of the region indicates the absolute size of the flow. It should be noted that the PS flows are a property of a flux surface, and thus, the values of E_r and the diamagnetic term at the considered radius are of importance. In the above equations it is assumed that n_α is constant on a flux surface. On top of these PS flows a parallel flow, $v_{B_\parallel}$, which is proportional to $B_\parallel$ can be added without violating the continuity equation on a flux surface. When the parallel dynamics within a flux surface is slow enough such that radial transport competes with it, the continuity equation does not require divergence free flows on each flux surface and poloidal asymmetries in particle densities might arise. In Fig. 1, the measurement locations of toroidal and poloidal (newly installed) rotation at the LFS are indicated along with the newly installed diagnostics for toroidal rotation at the HFS. The locations are well suited to see effects of PS flows.

Experiment In H-mode discharges, the LFS and HFS rotation at the plasma edge are recorded with 2-4 ms time resolution. The rotation measurements at the LFS are performed via CXRS at a heating beam. At the HFS, a D gas puff is applied which leads to CX reactions between the penetrating D gas cloud and the plasma impurities. With this method, information about rotation is obtained only in the outermost plasma region into which the neutrals penetrate, i.e a few cm. Two toroidal arrays of lines of sight (LOS) have been implemented at the HFS. One is looking directly at the gas puff and gathers the photons from the CX reactions (these LOSs are labeled with 'S' in Fig. 1) along with background photons that are emitted elsewhere on the path of the LOS. The second array views the periphery of the gas cloud (labeled 'B' in Fig. 1), and provides equivalent spectra without the CX signal such that the background signal in the spectra measured on the 'S' set of LOSs can be subtracted. It should be noted that in the following the measurements from LFS and HFS are denoted as toroidal rotation, however, the differences between parallel and toroidal velocities are very small due to the field line geometry - this systematic difference is typically smaller than the error bars which represent only the statistical uncertainty. The wavelength calibration is obtained by inter-shot measurements on a spectral lamp and is better than 1 km/s.

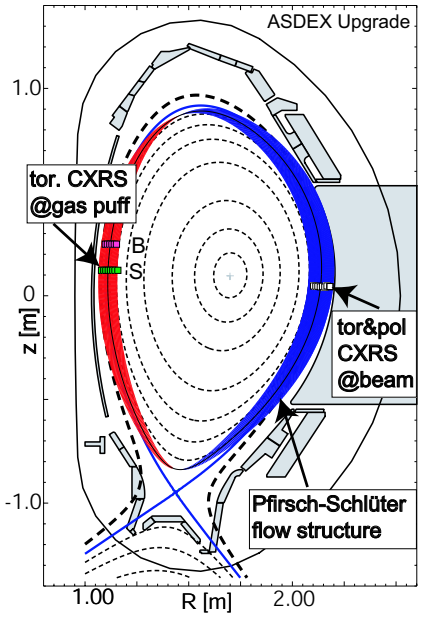

Fig. 1: *Structure of Pfirsch-Schlüter flows and diagnostic locations.*

At the LFS, the poloidal and toroidal CXRS measurements are used to obtain a profile of E_r. The alignment of the LFS CXRS data is performed by a comparison of the T_i-profile. The position of the separatrix is found by aligning the CXRS data to the electron profiles for which the separatrix position is known from power balance. The procedure is described in [2, 3, 4]. The HFS measurements are aligned to the LFS measurements (thus, also to the E_r data) using the T_i-profiles. The accuracy of the process is estimated to be higher than 2-3 mm. In Fig. 2(a), an alignment of the HFS T_i-profile w.r.t. to the LFS T_i-profile is presented. In Fig. 2(b), the toroidal rotation profiles are given. In this phase, the ELMs are small, high-frequency perturbations which have been induced by Ne-seeding. The latter allowed us to derive the rotation from Ne^{10+} and C^{6+} from the same spectrum (CX-lines at 524.897 nm (Ne) and 529.059 nm (C)). The profile described by the red data (C) agrees within the uncertainties with that obtained from the gray data (Ne) and both data sets exhibit an asymmetric behavior w.r.t. the toroidal rotation measured at the LFS. For the latter only C data is presented for clarity, as within the uncertainties the measurements are consistent (cf. [1]). For the Ne-seeding case, the ELMs could not be filtered

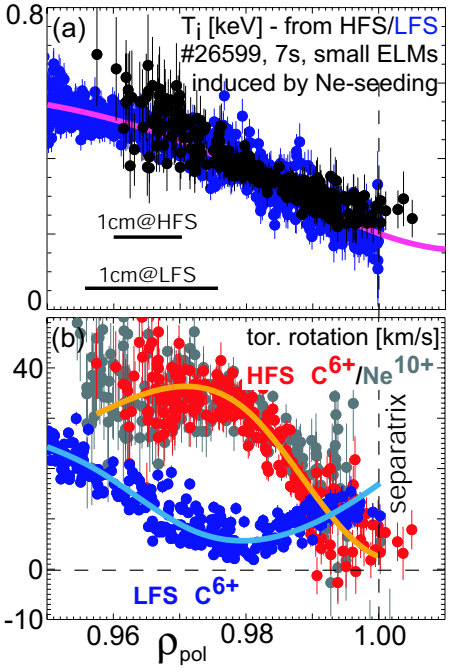

Fig. 2: *(a) HFS/LFS measurements of T_i to accomplish the alignment of the rotation profiles. (b) Toroidal/parallel rotation at HFS/LFS. The lines are spline fits to the data.*

out because of their high frequency, but their effect on the plasma is very small. A similar comparison of rotation velocities is presented in Fig. 3, for a type-I ELMy H-mode. The presented data originate from the second half of the ELM cycle, excluding the ELM crash. The discharge was repeated to obtain data for B^{5+} (494.467 nm) and for C^{6+}. The shapes of the edge rotation profiles are similar between the type-I and the Ne-seeding cases. For the latter case, the difference between the LFS and HFS rotation at about $\rho_{pol} = 0.975$ is larger by about 10 km/s than for the type-I case. For both cases, the LFS rotation increases and the HFS rotation decreases towards the separatrix, such that they cross over inside of the separatrix. These basic observations are valid even after shifting the profiles within the uncertainties of 2-3 mm.

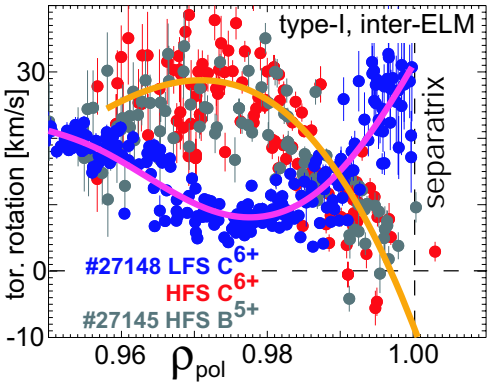

Fig. 3: *Toroidal/parallel rotation at HFS/LFS for C^{6+} and B^{5+}.*

Discussion In the following, the question of whether or not the observed flow velocities are consistent with a divergence free flow structure on a flux surface will be addressed. For this, the E_r measurements performed at the LFS, which will be described in detail at [5], are used. For the Ne-seeding case, E_r (black) is presented in Fig. 4(a). In Fig. 4(b), the predicted HFS rotation profiles are plotted, using the LFS measurements as inputs into Eq. 2. In order to predict $v_{\parallel,total}$ at the HFS, the LFS rotation is compared to $v_{\parallel,PS}$ (at the LFS) and the difference is attributed to $v_{B_\parallel}$ (at the LFS). Thus, $v_{B_\parallel}$ at the HFS is known by the ratio of the magnetic fields at the HFS and LFS, while $v_{\parallel,PS}$ at the HFS is evaluated by Eq. 2. The spline fit to the experimental data (orange), presented in Fig. 2(b), is compared to a prediction strictly based on Eq. 2 (magenta), where the diamagnetic term of the considered species (C^{6+}) is used. The magenta error bars indicate the propagated error due to a change of the toroidal rotation at the LFS by $\pm 5\mathrm{km/s}$, which corresponds to the scatter of the data around the spline fit. The measurement agrees with the prediction up to a radius of about $\rho_{pol} = 0.98$. For comparison the diamagnetic term of D (cf. Fig. 4(a)) is used to evaluate the PS flows of D (red in Fig 4(b)). These flows are of relevance, as there are indications that the impurities are dragged along in the D flows [1]. However, in Fig. 4(b) the measurement of the C/Ne flows at the HFS are clearly different from the expectations for D flows. At the separatrix, the measured C/Ne flows and the predicted D flows are similar, however, for the type-I ELM case (cf. Fig. 4(d)) this is not observed. This demonstrates that the impurity and D flows

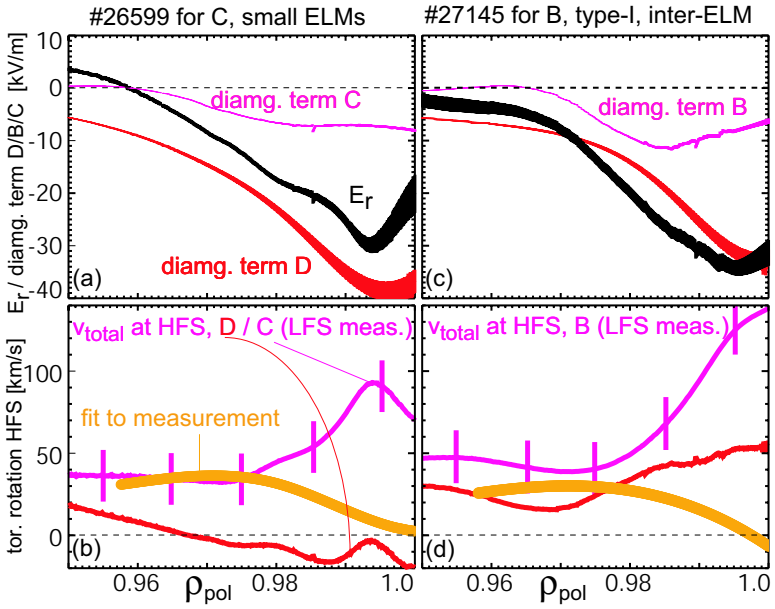

Fig. 4: *(a)/(c) E_r and diamg. terms of D/B/C, for #26599 / #27145. (b)/(d) Measurements and predictions for the rotation at the HFS.*

are not strongly coupled at the separatrix. Thus, outside of $\rho_{pol} = 0.98$ the measurement does not follow any of the calculated PS flows. For the inter-ELM phase in the type-I ELM case (Fig. 4(c) and 4(d)) similar observations are made. Due to the lower scatter in the data, the Ne-seeding case is better suited to argue about the HFS flows, however, as the type-I ELMy H-mode is a more common scenario it is presented along with the Ne-seeding data. The flows for the type-I ELMy H-mode demonstrated that the D-flow and the C/B-flows are different, which means that there should also be a difference between the flows of the various impurities. This difference is probably small compared to the scatter in the measurement. Future investigation will try to better quantify that difference.

In Fig. 5, typical time scales of the important processes are presented versus radius. When approaching the separatrix (i.e. outside of $\rho_{pol} = 0.98$), the time scale of radial transport to the SOL (black) becomes comparable to the parallel transit time (travel time from LFS to HFS at the ion sound speed, including electron drag) of D (red) and the impurity ions (orange). Additionally, the perpendicular velocity (here, E×B-velocity is used) is large at the pedestal such that the drift time from LFS to HFS (blue) becomes faster than the parallel transit time. For radial transport the time scales were estimated using a diffusion coefficient $D_\perp = 0.2\,\mathrm{m}^2/\mathrm{s}$, a value which is in agreement with the findings in [4]. This means that outside of $\rho_{pol} = 0.98$ radial transport is an important player, as the establishment of the flow equilibrium on a flux surface needs more time than the radial transport of particles to the SOL, where entirely different flows are known to exist. Thus, it is understandable that the PS flow structure is violated outside of $\rho_{pol} = 0.98$, and additionally also particle sources due to transport might become relevant for providing non-constant impurity densities on flux surfaces.

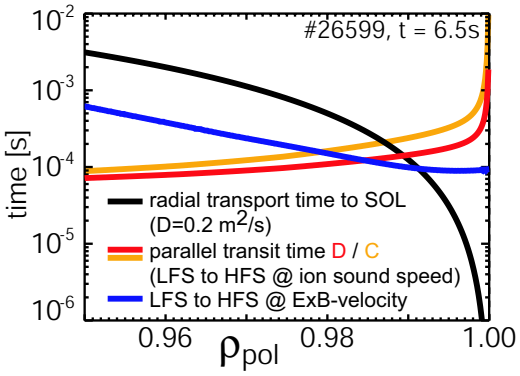

Fig. 5: *Comparison of relevant time scales.*

The importance of radial transport outside of $\rho_{pol} = 0.98$ is also acknowledged in [6, 7]. There, an influence of the scrape-off layer flows on the pedestal flows via viscosity is postulated. The respective B2 modeling exhibits similar structures of parallel flows as measured in [1]. It should be noted that in [8] (at Alcator C-Mod) a similar discrepancy between the expected and measured HFS flows was explained by the possible existence of a strong asymmetry in the impurity density (up to a factor of 3) on a flux surface. The asymmetry was required outside of about $\rho_{pol} = 0.98$. In [8] it was demonstrated that a redistribution of impurities due to neoclassical effects is not sufficient to explain the asymmetry. A direct measurement of the impurity density performed in [9] yielded an asymmetry of about a factor of 5. A direct analysis of the HFS impurity density profile is pending at ASDEX Upgrade, but such an effect would be also in line with the considerations on the relevant time scales as mentioned above.

References

[1] T. Pütterich *et al.*, PRL **102**, 025001 (2009)
[2] E. Wolfrum *et al.*, PPCF **51**, 124057 (9pp) (2009)
[3] J. Neuhauser *et al.*, PPCF **44**, 855 (2002)
[4] T. Pütterich *et al.*, JNM **In Press**, (2011)
[5] E. Viezzer, EFTSOMP 2011, Strasbourg (Satellite to EPS 2011)
[6] V. Rozhansky *et al.*, JNM **In Press**, (2011)
[7] V. Rozhansky *et al.*, JNM **363–365**, 664 (2007)
[8] K. D. Marr *et al.*, PPCF **52**, 055010 (2010)
[9] R. Churchill and B. Lipschultz, TP9.00065, 52nd APS, Chicago